21PM2A-04

Coherent Sub-Space Processing for Time Reversal Microwave Imaging

Md Delwar Hossain [#1], Ananda Sanagavarapu Mohan [#2]

[#] *Faculty of Engineering and IT, University of Technology Sydney (UTS)*
Sydney, NSW-2007, Australia

[1] Md.D.Hossain@student.uts.edu.au

[2] Ananda.Sanagavarapu@uts.edu.au

Abstract— **We consider electromagnetic inverse scattering using time reversal for microwave imaging for early stage breast cancer detection. Assuming that the malignant tissue inside the breast to be the strongest scatterer, we localize it by employing subspace based time reversal techniques viz., decomposition of the time reversal operator (DORT) and time reversal MUSIC. In denser breasts, the fibroglandular tissue clutter dominates the back scattered signals at the receiver. Also, the received scattered field becomes highly correlated thereby significantly affecting the performance of subspace based time reversal algorithms. To alleviate this, we employ coherent signal subspace transformation to obtain a coherently focussed time reversal operator (TRO). We test the performance of proposed method using MRI derived realistic numerical breast phantom of a moderately dense breast.**

I. INTRODUCTION

Solutions of inverse problems are of great significance in imaging which has many applications in non-destructive testing, surveillance, localization, as well as biomedical applications for diagnosis and treatment. Electromagnetic wave propagation through any medium depends on the complex dielectric properties of the medium. Whenever the electromagnetic wave experiences a discontinuity in its propagation path due either changes in medium dielectric profile or due to the presence of any object or scatterer, the incident wave field is scattered in different directions depending on the dielectric mismatch between the two objects, polarization, surface geometry etc. The solution of an electromagnetic inverse problem usually obtains the profile of a scattering object in terms of spatial coordinates, reflectivity, polarisation etc. for a given excitation and known the back scattering response.

Microwave imaging is a solution of electromagnetic inverse problem which has shown some promising potential for early detection of breast cancer. It mainly detects the presence or absence of a target tissue purely based on backscattering response from malignant lesions and surrounding breast tissues. Breast contains fatty, fibro connective and fibroglandular tissues and the dielectric property contrast between malignant lesions and other tissues determine the differences in the backscattering response that could be utilised for the cancer detection [1]. It is well established by now that the malignant breast lesion has the strongest backscattering response as compared to healthy fatty breast tissues and hence it can be localized using the solution of the corresponding inverse problem. However, recent studies indicated [1] that the presence of dense fibroglandular tissues can mask the back scattering from a malignant lesion due to lower dielectric contrast. In such dense breast scenarios, the solution of the corresponding inverse problem poses significant challenges. In this paper, we propose to employ coherently processed time reversal imaging techniques for solving the inverse scattering problem arising in the breast cancer detection.

TR based localization scheme was pioneered by M. Fink [2] for acoustics and later it was extended for electromagnetic fields [3]. Use of the TR method for breast cancer detection and localization has already been considered in a number of studies [4-9]. Time reversal method has also found application in microwave hyperthermia treatment process[10]. In iterative TR, the received backscattered field is iteratively back propagated to achieve focusing only on to the strongest scatterer. To obtain selective focusing on to multiple scatterers, DORT technique was later introduced [11], but it failed to separate two non-well resolved targets. To overcome these limitations, TR-MUSIC was introduced [12] that has very high resolution. Both DORT and TR-MUSIC are subspace based imaging techniques based on eigen value decomposition (EVD) of the time reversal operator (TRO) that utilize the signal subspace and noise subspace of the multistatic response matrix respectively. The breast is a highly cluttered medium containing different types of tissues. The scattered field received at different locations and frequencies can be highly correlated. Consequently DORT and TR-MUSIC exhibits higher uncertainties leading to poorer localisation performance. In this paper, we investigate use of coherent subspace signal processing to improve the focussing ability of DORT and TR-MUSIC methods when employed for cancer detection in highly cluttered breast phantoms. The proposed coherent signal subspace processing helps to construct coherently focussed TRO (C-TRO) [13] [14]. We investigate the effectiveness of the proposed technique using realistic MRI-derived breast phantoms [15].

We use FDTD to simulate the forward process that obtains the backscattered field from the breast tissues including the tumour. The received field is employed in the time reversal process with the aid of Green's function for estimating the location of the suspicious regions. The rest of the paper is organized as follows. In Section II we provide the formulation

of C-TRO along with DORT and TR-MUSIC. Section III includes the details of FDTD simulation with numerical breast phantom and the results are provided in section IV followed by conclusions in section V.

II. Inverse Scattering using Time Reversal

Let us consider a transceiver array of N elements located at $\mathbf{r}_n^t$, $n=1,2,...,N$. We assume that each antenna element consists of 3 small dipoles aligned along *x, y* and *z* axis having lengths of d^x, d^y and d^z respectively and are fed by driving currents J^x, J^y and J^z. There are M targets located at $\mathbf{r}_m^o$, $m=1,2,...,M$ with permittivity tensor given as

$$\bar{\bar{\boldsymbol{\varepsilon}}}_m = diag\{\varepsilon_1^x, \varepsilon_1^y, \varepsilon_1^z, \varepsilon_2^x, \varepsilon_2^y, ..., \varepsilon_M^z\} \quad (1)$$

For the case of isotropic targets $\varepsilon_m^x = \varepsilon_m^y = \varepsilon_m^z = \varepsilon_m$ where $m=1,2,...,M$. The incident electric field at a location $\mathbf{r}$ assuming non-magnetic medium can be obtained as

$$\mathbf{E}_{in}(\mathbf{r}) = \sum_{n=1}^{N} i\omega\mu_o \bar{\bar{\mathbf{G}}}(\mathbf{r}, \mathbf{r}_n^t)\mathbf{D}_n\mathbf{J}_n \quad (2)$$

where μ_o is the permeability of the background medium, $\mathbf{D}_n = diag\{d_n^x\ d_n^y\ d_n^z\}$, $\mathbf{J}_n = [J_n^x\ J_n^y\ J_n^z]^T$ and the dyadic Green's function for an unbounded homogeneous medium is defined as

$$\bar{\bar{\mathbf{G}}}(\mathbf{r}, \mathbf{r}') = \left(\bar{\bar{\mathbf{I}}} + \frac{\nabla\nabla}{k^2}\right)\exp^{jk|\mathbf{r}-\mathbf{r}'|/4\pi|\mathbf{r}-\mathbf{r}'|} \quad (3)$$

where k is the wave number of the medium. Hence the incident electric field can be represented in matrix form as follows

$$\mathbf{E}_{in} = \bar{\bar{\boldsymbol{\mathcal{G}}}}'^{T} \cdot \bar{\bar{\mathbf{D}}} \cdot \bar{\mathbf{J}} \quad (4)$$

where $(.)^T$ denotes transpose operation and

$$\bar{\bar{\boldsymbol{\mathcal{G}}}}' = \begin{bmatrix} i\omega\mu_o\bar{\bar{\mathbf{G}}}(\mathbf{r}_1^o, \mathbf{r}_1^t) & i\omega\mu_o\bar{\bar{\mathbf{G}}}(\mathbf{r}_2^o, \mathbf{r}_1^t) & ... & i\omega\mu_o\bar{\bar{\mathbf{G}}}(\mathbf{r}_M^o, \mathbf{r}_1^t) \\ i\omega\mu_o\bar{\bar{\mathbf{G}}}(\mathbf{r}_1^o, \mathbf{r}_2^t) & i\omega\mu_o\bar{\bar{\mathbf{G}}}(\mathbf{r}_2^o, \mathbf{r}_2^t) & ... & i\omega\mu_o\bar{\bar{\mathbf{G}}}(\mathbf{r}_M^o, \mathbf{r}_2^t) \\ \vdots & \vdots & \ddots & \vdots \\ i\omega\mu_o\bar{\bar{\mathbf{G}}}(\mathbf{r}_1^o, \mathbf{r}_N^t) & i\omega\mu_o\bar{\bar{\mathbf{G}}}(\mathbf{r}_2^o, \mathbf{r}_N^t) & & i\omega\mu_o\bar{\bar{\mathbf{G}}}(\mathbf{r}_M^o, \mathbf{r}_N^t) \end{bmatrix} \quad (5)$$

$$\bar{\bar{\mathbf{D}}} = diag\{d_1^x, d_1^y, d_1^z, d_2^x, d_2^y, ..., d_N^z\} \quad (6)$$

$$\bar{\mathbf{J}} = [J_1^x\ J_1^y\ J_1^z\ J_2^x\ J_2^y\ ...\ J_N^z]^T \quad (7)$$

The multistatic matrix is formed by sequentially transmitting a waveform from each element of the array and the resulting scattered field is received by all the elements of the array. The scattered field received at j-th antenna due to excitation at l-th antenna can be represented as [15]

$$\mathbf{E}_{jl}^s(\mathbf{r}_j^t) = \sum_{m=1}^{M}\int_{\upsilon_m} \bar{\bar{\mathbf{G}}}(\mathbf{r}_j^t, \mathbf{r}_m^o)\left[k_m^2(\mathbf{r}_m^o) - k^2\right]\bar{\bar{\mathbf{G}}}(\mathbf{r}_m^o, \mathbf{r}_l^t)\mathbf{E}_t(\mathbf{r}_m^o)d\mathbf{r}_m^o \quad (8)$$

here υ_m is volume of the m-th scatterer, $\mathbf{E}_t(\mathbf{r}_m^o)$ is the total field incident on the target at $\mathbf{r}_m^o$, and $\left[k_m^2(\mathbf{r}_m^o) - k^2\right]$ represents the dielectric contrast between the target and the medium where

$$k_m^2(\mathbf{r}_m^o) = \begin{cases} diag\{\omega^2\mu_o\varepsilon_m^x(\mathbf{r}), \omega^2\mu_o\varepsilon_m^y(\mathbf{r}), \omega^2\mu_o\varepsilon_m^z(\mathbf{r})\}, & \mathbf{r} \in \upsilon_m \\ diag\{k^2, k^2, k^2\}, & \mathbf{r} \notin \upsilon_m \end{cases} \quad (9)$$

Considering the targets are small the multistatic matrix is obtained as

$$\mathbf{K} = \bar{\bar{\boldsymbol{\mathcal{G}}}}\bar{\bar{\boldsymbol{\zeta}}}\bar{\bar{\boldsymbol{\mathcal{G}}}}^T \quad (10)$$

where $\bar{\bar{\boldsymbol{\mathcal{G}}}} = \bar{\bar{\boldsymbol{\mathcal{G}}}}'/i\omega\mu_o$ and $\bar{\bar{\boldsymbol{\zeta}}}$ is a $3M\times3M$ matrix defined as follows

$$\bar{\bar{\boldsymbol{\zeta}}} = diag\{\omega^2\mu_o\varepsilon_1^x - k^2, \omega^2\mu_o\varepsilon_1^y - k^2, ..., \omega^2\mu_o\varepsilon_M^z - k^2\} \quad (11)$$

The problem is simplified for 2D scenario using TM-z polarization where only z-component of the electric field exists and the antennas become infinite line sources along z-axis. For 2D TM-z polarization the dyadic $\bar{\bar{\mathbf{G}}}$ reduces to $G(\mathbf{r}, \mathbf{r}', \omega) = \frac{1}{4j}H_0^1(k|\mathbf{r}-\mathbf{r}'|)$ where, H_0^1 is the 0-th order Hankel function of type *1*. Then the multistatic matrix can be written as

$$\mathbf{K} = \boldsymbol{\mathcal{G}}\boldsymbol{\Gamma}\boldsymbol{\mathcal{G}}^T \quad (12)$$

where, $\boldsymbol{\Gamma} = diag\{\Gamma_1^z, \Gamma_2^z, \ ...\ , \Gamma_m^z\}$ represents the effective scattering strengths of the targets and $\boldsymbol{\mathcal{G}}$ is obtained as follows

$$\boldsymbol{\mathcal{G}} = [\mathbf{g}(\mathbf{r}_1^o)\quad \mathbf{g}(\mathbf{r}_2^o)\quad ...\quad \mathbf{g}(\mathbf{r}_m^o)] \quad (13)$$

In (13) the Green's function vector is given as

$$\mathbf{g}(\mathbf{r}, \omega) = \left[G(\mathbf{r}, \mathbf{r}_1^t, \omega), \cdots, G(\mathbf{r}, \mathbf{r}_N^t, \omega)\right]^T \quad (14)$$

The rank of the multistatic matrix $\mathbf{K}$ is obtained as

$$r_k \le \min(M, N) \quad (15)$$

In order to unambiguously identify each target we require that the number of targes to be smaller than the number of antenna elements in the array.

A. Coherent Time Reversal Operator

The TRO that includes combination of forward propagation, TR process and back propagation is given by

$$\mathbf{T} = \mathbf{K}^H\mathbf{K} \quad (16)$$

where $(.)^H$ denotes hermitian transpose. The rank of the TRO matrix $\mathbf{T}$ is at most equal to the number of scatterers. Using singular value decomposition (SVD) $\mathbf{T}$ can be expressed as

$$\mathbf{T} = \mathbf{U}(\omega)\boldsymbol{\Phi}(\omega)\mathbf{V}(\omega) \quad (17)$$

where $\mathbf{U}$ and $\mathbf{V}$ contains the left and right singular vectors and $\boldsymbol{\Phi}$ contains the singular values of $\mathbf{T}$.

When UWB excitation is used, the scattered field is recorded in the time domain which is later fourier transformed to obtain the TRO in the frequency domain for discrete frequency bins. It is possible to transfer the TRO from different frequency bins to into a single focussed entity that will form a coherently focussed-TRO (or C-TRO). In highly cluttered environments, the resulting multiple scattering could result in highly correlated signals, thus leading to poor performance of subspace based TR techniques. Hence it is necessary to incorporate methods to de-correlate the C-TRO. If we could transform the C-TRO into a unitary matrix, it will

ensure that the signals are decorrelated. Towards that end, we first obtain the unitary focusing matrix, **W** as [13]

$$\min_{\mathbf{W}(\omega_f)} \left\| \mathbf{K}(\omega_o) - \mathbf{W}(\omega_f)\mathbf{K}(\omega_f) \right\|_F \quad (18)$$

where $\|.\|_F$ denotes the Frobenius norm and ω_f denotes f-th frequency bin of **T** given by (17). The minimization problem in (18) has the solution [13]

$$\mathbf{W}(\omega_f) = \mathbf{V}(\omega_f)\mathbf{U}^*(\omega_f) \quad (19)$$

where $(.)^*$ denotes conjugate operation. Since, **U** and **V** are both unitary matrices, **W** is also a unitary matrix. Finally, we obtain the coherently focussed TRO as

$$\hat{\mathbf{T}}(\omega_o) = \sum_{f=1}^{F} \mathbf{W}(\omega_f)\mathbf{T}(\omega_f)\mathbf{W}^*(\omega_f) \quad (20)$$

Thus, the energy collected from a total of F frequency bins will be condensed into the C-TRO [13]. Thus, estimating $\hat{\mathbf{T}}$ and using it instead of **T** at each frequency bin would result in improved imaging performance.

B. TR-MUSIC Imaging with coherent TRO:

The vector space, $\mathcal{C}^N$ of the estimated C-TRO, $\hat{\mathbf{T}}$ can be decomposed into signal subspace, $\mathcal{S}$ and noise subspace, $\mathcal{N}$ where $\mathcal{S}$ and $\mathcal{N}$ are orthogonal to each other if the number of targets is smaller than the number of antenna elements. The Green's function vectors of the background medium form the ortho-normal bases of the signal subspace. Signal subspace, $\mathcal{S}$ is spanned by the eigen vectors with significant eigen values. Similarly noise subspace, $\mathcal{N}$ is spanned by the eigen vectors with zero eigen values. So, when **r** coincides with actual target

$$\sum_{\Phi_m=0} \left| \mathbf{v}_m{}^H g(\mathbf{r}) \right| = 0 \quad (21)$$

where, $\mathbf{v}_m$ is the m-th eigen vector of $\hat{\mathbf{T}}$. Hence the TR-MUSIC pseudospectrum with C-TRO is constructed as given below.

$$I(\mathbf{r})_{TR-MUSIC} = \frac{1}{\sum_{\Phi_m=0} \left| \mathbf{v}_m{}^H g(\mathbf{r}) \right|^2} \quad (22)$$

C. DORT Imaging with coherent TRO:

DORT uses signal subspace for imaging. For well resolved targets, each eigen vector in signal subspace is associated with a target that is embedded within a background. Hence, when the eigen vectors are backpropagated using the Green's function of the medium, the target location can be obtained. If more than one target is present, it is possible to selectively focus onto each one of them using the corresponding eigen vectors. The DORT imaging functional with coherent time reversal operation is given by

$$I(\mathbf{r})_{DORT} = \sum_{\Phi_m>0} \left| \mathbf{v}_m{}^H g(\mathbf{r}) \right|^2 \quad (23)$$

III. Forward Problem Simulation

The first step is to obtain the backscattered response from the breast tissues. We solve the forward problem through FDTD simulation using a MRI derived realistic numerical moderately dense breast phantom (C3 model) which is obtained from UWCEM breast phantom repository [16]. A 2-D slice of the C3 breast model is shown in Fig. 1. The single pole debye parameters are provided in Table I [1, 17]. We consider that a malignant lesion with a maximum diameter of 10mm is embedded inside the phantom whose location is indicated by the white circle in Fig. 1.

The phantom is excited with a differentiated Gaussian pulse that has a centre frequency 4.5GHz and -3dB bandwidth 5GHz. The FDTD grid size is 0.5mm in all directions. A 21element receive array is used to record the backscattered field from the breast phantom. In order to reduce the reflection from skin, a matching liquid is used in which the phantom and the antenna array are immersed. It is assumed that the breast phantom is placed on the *xy*-plane and the incident field is TM-z polarized and hence the antenna elements are ideal infinite line sources along *z*-axis.

TABLE I

Single-Pole Cole-Cole Parameters for the Dielectric Properties of Different Breast Tissues

Tissue Type	ε_∞	$\Delta\varepsilon$	τ(ps)	α	σ_s(S/m)
Adipose-low	2.908	1.200	16.88	0.069	0.020
Adipose-Medium	3.140	1.708	14.65	0.061	0.036
Adipose-High	4.031	3.654	14.12	0.055	0.083
Glandular-Low	9.941	26.600	10.90	0.003	0.462
Glandular-Medium	7.821	41.480	10.66	0.047	0.713
Glandular-High	6.151	48.260	10.26	0.049	0.809
Transitional	6.987	15.127	12.51	0.025	0.272
Skin	15.30	24.800	15.00	0.003	0.740
Tumor	9.058	51.310	10.84	0.022	0.899

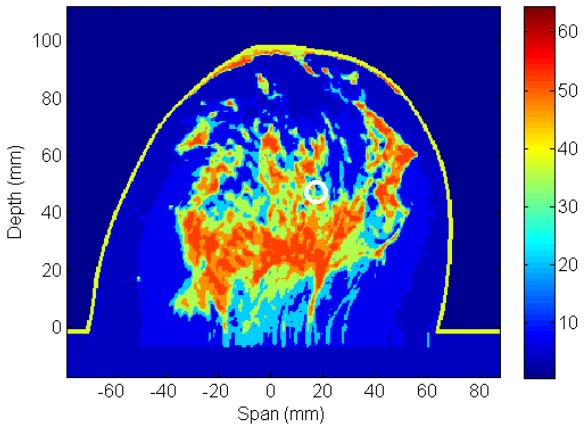

Fig. 1. MRI based numerical C3 breast phantom.

IV. Results

The scattered field obtained from the FDTD simulation is used for imaging. We first use conventional TRO "**T**" for DORT and TR imaging to obtain images as shown in Figs. 2-3. Then we estimate the C-TRO given by $\hat{\mathbf{T}}$ to use it with DORT and TR-MUSIC by combining the information in different frequency bins to form the images as shown in Figs. 4-5. The true tumor location is indicated using a small white

circle. The distribution of first seven singular values obtained for conventional TRO and proposed C-TRO are illustrated in Figs. 6-7.

It is observed from the DORT images that the highest intensity is closer to the actual tumor location. We also observe a very wide side lobe in DORT image when conventional TRO is employed as shown in Fig 2. The images formed using TR-MUSIC with conventional TRO, on the other hand, exhibits several peaks, some around the actual tumor location and the other away from it indicating the location ambiguity. On the other hand, the DORT image obtained with the proposed C-TRO shows the estimated location very close to the true tumor location and further, has significantly reduced the side lobes. Similar improvements can also be observed for TR-MUSIC imaging that employs C-TRO, although issues of false peaks still prevail. Further, the effects of C-TRO processing can readily be observed by inspecting the singular values in Figs 6-7. The second and subsequent singular values have decreased by almost 20% as a result of proposed coherent signal subspace transformation.

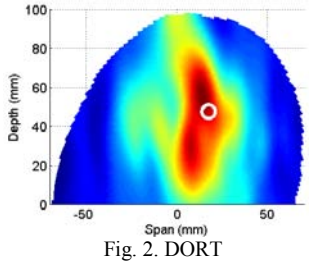

Fig. 2. DORT

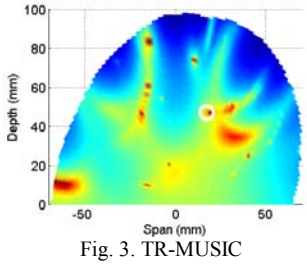

Fig. 3. TR-MUSIC

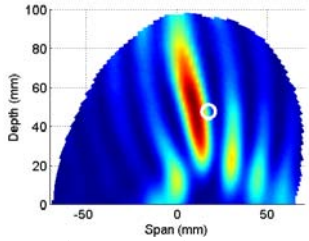

Fig. 4. DORT for C-TRO

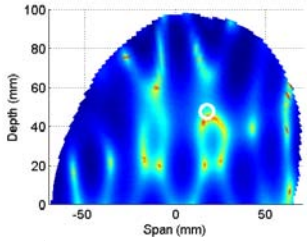

Fig. 5. TR-MUSIC for C-TRO

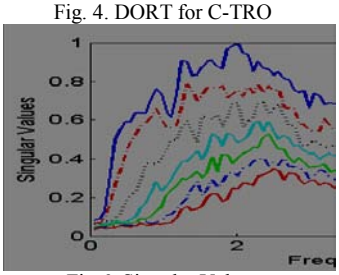

Fig 6. Singular Values

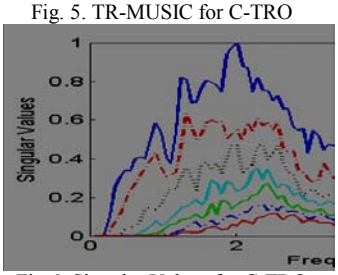

Fig 6. Singular Values for C-TRO

V. Conclusions

The results indicate the coherently focused time reversal operator (C-TRO) has significantly enhanced the contribution of dominant singular values which has resulted in reduced side lobes of images formed by DORT and TR-MUSIC. The proposed methods also accurately estimate the location of tumor in a moderately dense breast phantom. It is evident that by using the coherent signal subspace transformation reduces the degree of signal correlation which is useful in breast cancer detection in the presence of dense glandular tissues. In addition, use of C-TRO also results in faster processing as imaging operation is not required to be carried out at each frequency bin. Thus, it is possible to obtain better estimation of the tumor location with improved resolution and reduced computational burden.

Acknowledgment

The work reported in this paper is supported by the Australian Research Council through a Discovery Grant DP 0773234.

References

[1] M. Lazebnik, et.al., "A large-scale study of the ultrawideband microwave dielectric properties of normal, benign and malignant breast tissues obtained from cancer surgeries," *Phys. Med. Biol.,* vol. 52, pp. 6093-6115, 2007.

[2] M. Fink, "Time reversal of ultrasonic fields. I. Basic principles," *IEEE Trans. Ultras. Ferroel. Freq. Contr.,* vol. 39, pp. 555-566, 1992.

[3] L. Dehong, et.al., "Electromagnetic time-reversal imaging of a target in a cluttered environment,", *IEEE Trans. Ant. Propag.,* vol. 53, pp. 3058-3066, 2005.

[4] P. Kosmas and C. M. Rappaport, "Time reversal with the FDTD method for microwave breast cancer detection," *IEEE Trans. Microw. Theo. Tech.,* vol. 53, pp. 2317-2323, 2005.

[5] P. Kosmas and C. M. Rappaport, "FDTD-based time reversal for microwave breast cancer Detection-localization in three dimensions," *IEEE Trans. Microw. Theo. Tech.,* vol. 54, pp. 1921-1927, 2006.

[6] Y. Chen, et.al., "Pulse Design for Time Reversal Method as Applied to Ultrawideband Microwave Breast Cancer Detection: A Two-Dimensional Analysis," *IEEE Trans. Ant. Propag.,* vol. 55, pp. 194-204, 2007.

[7] P. Kosmas, "Application of the DORT technique to FDTD-based time reversal for microwave breast cancer detection," in Proc. *European Microwave Conference(EUMC),* Munich, Germany, 9-12 October, 2007, pp. 306-308.

[8] J. Yuanwei, J. Yi, and J. M. F. Moura, "Time Reversal Beamforming for Microwave Breast Cancer Detection," in Proc. *IEEE International Conference on Image Processing (ICIP),* Texas, USA, 16-19 September, 2007, pp. V-13-V-16.

[9] C. Yifan, et.al., "Time-Reversal Ultrawideband Breast Imaging: Pulse Design Criteria Considering Multiple Tumors With Unknown Tissue Properties," *IEEE Trans. Ant. Propag.,* vol. 56, pp. 3073-3077, 2008.

[10] H. D. Trefná, J. Vrba, and M. Persson, "Time-reversal focusing in microwave hyperthermia for deep-seated tumors," *Phys. Med. Biol.,* vol. 55(8), pp. 2167-2185, April 2010.

[11] C. Prada, S. Manneville, D. Spoliansky, and M. Fink, "Decomposition of the time reversal operator: Detection and selective focusing on two scatterers," *J. Acoust. Soc. Am.,* vol. 99, pp. 2067-2076, 1996.

[12] A. J. Devaney, "Time reversal imaging of obscured targets from multistatic data," *IEEE Trans. Ant. Propag.,* vol. 53, pp. 1600-1610, 2005.

[13] H. Hung and M. Kaveh, "Focussing matrices for coherent signal-subspace processing," *IEEE Trans. Acoust. Speech Sig. Proces.,* vol. 36, pp. 1272-1281, 1988.

[14] W. Zhisong, L. Jian, and W. Renbiao, "Time-delay- and time-reversal-based robust capon beamformers for ultrasound imaging," *IEEE Trans. Med. Imag.,* vol. 24, pp. 1308-1322, 2005.

[15] L. Tsang and J. A. Kong, Scattering of Electromagnetic Waves: Advanced Topics: John Wiley & Sons, Inc., 2001.

[16] Available: http://uwcem.ece.wisc.edu/MRIdatabase/index.html

[17] E. Zastrow, et.al., "Development of Anatomically Realistic Numerical Breast Phantoms With Accurate Dielectric Properties for Modeling Microwave Interactions With the Human Breast," IEEE Trans. Biomed. Eng. , vol. 55, pp. 2792-2800, 2008.